Synthesis, Structures, and Magnetic Properties of Fe_2, Fe_{17}, and Fe_{19} Oxo-Bridged Iron Clusters: The Stabilization of High Ground State Spins by Cluster Aggregates

A. K. Powell,*,† S. L. Heath,† D. Gatteschi,*,‡ L. Pardi,‡ R. Sessoli,‡ G. Spina,§ F. Del Giallo,|| and F. Pieralli||

Contribution from the School of Chemical Sciences, University of East Anglia, Norwich, Norfolk, NR4 7TJ, U.K., Dipartimento di Chimica, Universita degli Studi di Firenze, Via Maragliano 77, 50144 Firenze, Italy, Dipartimento di Fisica, Universita degli Studi di Firenze, Piazzale E. Fermi 2, Firenze, Italy, and the I.R.O.E.-C.N.R., Firenze, Italy

Received February 14, 1994[⊗]

Abstract: The compound $[Fe(heidi)(H_2O)]_2$, where $H_3heidi = N(CH_2COOH)_2(CH_2CH_2OH)$, crystallizes in a triclinic space group $P\bar{1}$, with $a = 6.838(1)$ Å, $b = 7.058(1)$ Å, $c = 9.676(2)$ Å, $\alpha = 103.29(1)°$, $\beta = 93.58(1)°$, $\gamma = 97.83(1)°$ and is a dinuclear iron(III) compound with the two iron atoms linked by the alkoxide function of the ligand. The dinucleating ability of this ligand is also present in the two polyiron(III) oxyhydroxide cluster compounds $[Fe_{19}(\mu_3\text{-}O)_6(\mu_3\text{-}OH)_6(\mu_2\text{-}OH)_8(heidi)_{10}(H_2O)_{12}]^{1+}$ and $[Fe_{17}(\mu_3\text{-}O)_4(\mu_3\text{-}OH)_6(\mu_2\text{-}OH)_{10}(heidi)_8(H_2O)_{12}]^{3+}$ which crystallize in the same unit cell together with 60 lattice waters and four nitrate anions in the triclinic space group $P\bar{1}$, with $a = 12.693(13)$ Å, $b = 18.060(17)$ Å, $c = 28.784(15)$ Å, $\alpha = 93.66(6)°$, $\beta = 94.95(6)°$, $\gamma = 89.88(8)°$. These clusters contain trapped iron hydroxide mineral portions produced by a modified hydrolysis of iron(III) in the presence of the ligand. They are the largest polyiron(III) oxyhydroxide clusters synthesized to date. A detailed investigation of their magnetic properties using ac and dc susceptibility measurements and EPR and Mössbauer spectroscopies reveals that in at least one of the clusters the ground state spin cannot be smaller than $S = {}^{33}/_2$, the largest spin ground state so far observed in a molecular cluster.

Introduction

Iron is ubiquitous in Nature, particularly in the form of iron(III) species, and as water is the principal solvent existing in both organisms and the natural environment, the hydrolytic chemistry of iron(III) is of special relevance. In addition, such media contain or are in contact with ligating groups, *e.g.*, on small molecules such as citrate, humic acids, *etc.*, and protein side chains.[1] In recognition of this we have been using chelating ligands containing carboxylate functions and other functionalities in order to determine which parameters are important in controlling the speciation of iron. We have found that by using the ligand heidi [($H_3heidi = N(CH_2COOH)_2(CH_2CH_2OH)$] in different controlled hydrolysis reactions of iron(III) two different compounds, $[Fe(heidi)(H_2O)]_2$ (**1**) and $[Fe_{19}(\mu_3\text{-}O)_6(\mu_3\text{-}OH)_6(\mu_2\text{-}OH)_8(heidi)_{10}(H_2O)_{12}]$ $[Fe_{17}(\mu_3\text{-}O)_4(\mu_3\text{-}OH)_6(\mu_2\text{-}OH)_{10}(heidi)_8(H_2O)_{12}]$ $(NO_3)_4{\cdot}60H_2O$ (**2**) can be obtained.[2] We wish to report here the full X-ray structural details and synthetic strategy used in preparing these compounds, in addition to their magnetic properties.

Other examples of polyiron clusters containing bridging oxygen centers are Fe_6,[3] Fe_8,[4] Fe_{10},[5] Fe_{11},[6] Fe_{12},[7] $Fe_{16}M$.[8] One of the fascinating aspects of the investigation of large iron clusters is that of providing models for the biomineralization of iron, which leads to such diverse compounds as ferritin and magnetite.[9] The recent discovery that magnetite is also present in the human brain has certainly added interest in this area.[10]

However, there are further aspects to the study of iron clusters since they are inherently magnetic, and when they assume the dimensions of nanoscale particles they may display novel properties intermediate between those of simple paramagnets and bulk magnets.[11,12] For example, superparamagnetic behavior has been reported for Fe_{12} clusters on the basis of Mössbauer

† University of East Anglia.
‡ Dipartimento di Chimica, Universita degli Studi di Firenze.
§ Dipartimento di Fisica, Universita degli Studi di Firenze.
|| I.R.O.E.-C.N.R.
⊗ Abstract published in *Advance ACS Abstracts*, February 1, 1995.

(1) Crichton, R. R. In *Inorganic Biochemistry of Iron Metabolism*; Horwood: New York, 1991.
(2) Heath, S. L.; Powell, A. K. *Angew. Chem., Int. Ed. Engl.* **1992**, *31*, 191.
(3) (a) Gerebleu, N. V.; Batsanov, A. S.; Timko, G. A.; Struchkov, Y. T.; Indrichan, K. M.; Popovich, G. A. *Dokl. Akad. Nauk SSSR* **1987**, *293*, 122. (b) Micklitz, W.; Lippard, S. J. *Inorg. Chem.* **1988**, *27*, 3067. (c) Micklitz, W.; Bott, S. G.; Bentsen, J. G.; Lippard, S. J. *J. Am. Chem. Soc.* **1989**, *111*, 372. (d) Hegetschweiler, K.; Schmalle, H.; Streit, H. M.; Schneider, W. *Inorg. Chem.* **1990**, *29*, 3625. (e) McCusker, J. K.; Christmas, C. A.; Hagen, P. M.; Chadha, R. K.; Harvey, D. F.; Hendrickson, D. N. *J. Am. Chem. Soc.* **1991**, *113*, 6114. (f) Hegetschweiler, K.; Schmalle, H. W.; Streit, H. M.; Gramlich, V.; Hund, H.-U.; Erni, I. *Inorg. Chem.* **1992**, *31*, 1299. (g) Nair, V. S.; Hagen, K. S. *Inorg. Chem.* **1992**, *31*, 4048. (h) Harding, C. J.; Henderson, R. K.; Powell, A. K. *Angew. Chem., Int. Ed. Engl.* **1993**, *32*, 570.
(4) (a) Wieghardt, K.; Pohl, K.; Jibril, I.; Huttner, G. *Angew. Chem., Int. Ed. Engl.* **1984**, *23*, 77. (b) Delfs, C.; Gatteschi, D.; Pardi, L.; Sessoli, R.; Wieghardt, K.; Hanke, D. *Inorg. Chem.* **1993**, *32*, 3099.
(5) Taft, K. L.; Lippard, S. J. *J. Am. Chem. Soc.* **1990**, *112*, 9629.
(6) Gorun, S. M.; Papaefthymiou, G. C.; Frankel, R. B.; Lippard, S. J. *J. Am. Chem. Soc.* **1987**, *109*, 3337.
(7) Taft, K. L.; Papaefthymiou, G. C.; Lippard, S. J. *Science* **1993**, *259*, 1302.
(8) Micklitz, W.; Lippard, S. J. *J. Am. Chem. Soc.* **1989**, *111*, 6856.
(9) (a) Harrison, P. M.; Artymiuk, P. J.; Ford, G. C.; Lawson, D. M.; Smith, J. M. A.; Treffry, A.; White, J. L. In *Biominealization: Chemical and Biochemical Perspectives*; Mann, S., Webb, J., Williams, R. J. P., Eds.; VCH: New York, 1989; p 257. (b) Mann, S.; Frankel, R. B. In *Biomineralization: Chemical and Biochemical Perspectives*; Mann, S., Webb, J., Williams, R. J. P., Eds.; VCH: New York, 1989; p 389. (c) Artymiuk, P. J.; Bauminger, E. R.; Harrison P. M.; Lawson, D. M.; Nowik, I.; Treffy, A.; Yewdell, S. J. In *Iron Biominerals*; Frankel, R. B., Blakemore, R. P., Eds.; Plenum: New York, 1991; p 269.
(10) Kirshvink, J. L.; Kobayashi-Kirschvink, A.; Woodford, B. *Proc. Natl. Acad. Sci. U. S. A.* **1992**, *89*, 7863.

0002-7863/95/1517-2491$09.00/0

data,[7] and it was suggested that the onset of bulk behavior is bound to the shape of the clusters; those which resemble small pieces of three-dimensional lattices show these properties earlier than those which have essentially flat or linear shapes.[13]

Experimental Section

Materials and Methods. All reagents were obtained from the Aldrich Chemical Company and used without further purification. Fourier transform infrared spectra were obtained as KBr disks on a Mattson Galaxy spectrometer. X-ray powder diffraction patterns for comparative purposes were measured on a Phillips PW1710 diffractometer equipped with Cobalt Kα radiation and an iron filter. The samples were prepared as finely ground powders and placed in the beam as a thin layer held in place on Sellotape or Vaseline.

[Fe(heidi)(H_2O)]$_2$ (1). First, 0.88 g (5 mmol) of the ligand H_3heidi (H_3heidi = $N(CH_2COOH)_2(CH_2CH_2OH)$ was dissolved in a 0.5 M sodium hydroxide solution (0.40 g, 10 mmol) in distilled water (20 mL). This solution was then added with stirring to a solution of iron(III) nitrate nonahydrate (2.02 g, 5 mmol) in distilled water (20 mL). The resultant solution had an initial pH of 1.38 and was light brown in color. Green crystals of [Fe(heidi)(H_2O)]$_2$ formed after 1 day, yield ca. 0.82 g (66.1% based on Fe). Anal. Found: C, 29.3; H, 4.1; N, 5.4; Fe, 22.7. $C_{12}H_{20}N_2O_{12}Fe_2$ requires: C, 29.4; H, 4.5; N, 5.7; Fe, 22.8.

[$Fe_{19}(\mu_3$-O)$_6(\mu_3$-OH)$_6(\mu_2$-OH)$_8$(heidi)$_{10}(H_2O)_{12}$] [$Fe_{17}(\mu_3$-O)$_4(\mu_3$-OH)$_6(\mu_2$-OH)$_{10}$(heidi)$_8(H_2O)_{12}$](NO_3)$_4$·60H_2O (2). In a typical experiment 0.44 g (2.5 mmol) of the ligand H_3heidi was dissolved in distilled water (20 mL) containing 6 equiv (1.22 mL, 15 mmol) of pyridine. This solution was then added with stirring to a solution of iron(III) nitrate nonahydrate (2.02 g, 5 mmol) in distilled water (20 mL). The resultant solution had an initial pH of 2.60 and was brown in color. Very small brown crystals of the compound formed after approximately 1 h in a yield of ca. 0.76 g (40% based on Fe). Anal. Found: C, 16.9; H, 4.4; N, 4.3; Fe, 26.5. $C_{108}H_{332}Fe_{36}N_{22}O_{226}$ requires; C, 17.1; H, 4.4; N, 4.1; Fe, 26.6.

X-ray Crystallography. The details of the data collection for the structures **1** and **2** are given in Table 1. Data collection for **1** was straightforward. For **2** several problems were encountered. **2** invariably crystallizes in the form of rather small crystals in a triclinic crystal system. The asymmetric unit contains two half-clusters plus a large amount of disordered lattice water and the nitrate counterions, resulting in the asymmetric unit containing over 200 non-hydrogen atoms (see below). All this leads to rather weak scattering of the X-rays, which made it necessary to collect data for 4 weeks on a conventional X-ray source in order to obtain enough significant reflections for structure solution and refinement.

Magnetic Measurements. Solid state magnetic susceptibility measurements in the temperature range 2−290 K were obtained with a Metronique MSO2 SQUID magnetometer. The data were corrected for the diamagnetic contribution estimated through the Pascal constants. No temperature-independent paramagnetism correction was taken into account.

Measurements on **2** below 80 K were performed in a weak field (H = 500 Oe) to avoid saturation effects.

AC susceptibility of **2** in zero applied field was measured on a home-assembled susceptometer down to 1.5 K at the operating frequency of 500 Hz.

EPR spectra of polycrystalline samples were recorded in the 4.2−300 K temperature range by using a VARIAN E9 spectrometer equipped with an Oxford Instruments continuous flow ESR9 cryostat.

Standard transmission Mössbauer measurements were taken using a Rh matrix source. The sample was cooled by a liquid He cryostat

(11) (a) Stamp, P. C. E.; Chudnowsky, E. M.; Barbara, B. *Int. J. Mod. Phys. B* **1992**, *9*, 1355. (b) Awschalom, D. D.; McCord, M. A.; Grinstein, G. *Phys. Rev. Lett.* **1990**, *65*, 783. (c) Ziolo, R. F.; Giannelis, E. P.; Weinstein, B. A.; O'Horo, M. P.; Ganguly, B. N.; Mehrotra, V.; Russell, M. W.; Huffman, D. R. *Science* **1992**, *257*, 219.

(12) (a) Delfs, C.; Gatteschi, D.; Pardi, L. *Comments Inorg. Chem.* **1993**, *15*, 27. (b) Gatteschi, D.; Pardi, L.; Barra, A. L.; Müller, A.; Döring, J. *Nature* **1991**, *354*, 463.

(13) Papaefthymiou, G. C. *Phys. Rev. B* **1992**, *46*, 10366.

Table 1. Crystallographic Information for **1** and **2**

	[Fe(hdidi)(H_2O)]$_2$ (**1**)
empirical formula	$C_{12}H_{20}N_2O_{12}Fe_2$
formula weight	495.99
crystal color, habit	green, cuboid
crystal dimensions (mm)	0.18 × 0.25 × 0.25
crystal system	triclinic
lattice parameters	
a	6.838(1) Å
b	7.058(1) Å
c	9.676(2) Å
α	103.29(1)°
β	93.58(1)°
γ	97.83(1)°
volume	448.1 Å^3
space group	$P\bar{1}$ (No. 2)
Z value	1
D_{calc}	1.838 g/cm^3
F(000)	254
μ(Mo Kα)	1.719 mm^{-1}
radiation	Mo Kα (λ = 0.71073 Å)
temperature	22 °C
scan type	ω
index ranges	0 → 9 *h*, −9 → 9 *k*, −12 → 12 *l*
no. of reflns measd	total 1903 (R_{int} = 0.0156)
	unique 1748
corrections	Lorentz-polarization
	empirical absorption
	(trans. factors 0.793−1.189)
system used	Siemens SHELXTL PLUS (VMS)
structure solution	Patterson method
refinement	full-matrix least-squares
function minimized	$\sum w(\|F_o\| - \|F_c\|)^2$
hydrogen atoms	riding model, fixed isotropic *U*
weighting scheme	$w^{-1} = \sigma^2(F) + 0.00062F^2$
no. observns ($F > 6.00\sigma(F)$)	1659
refln/parameter ratio	10.57:1
residuals: *R*; wR	0.0351, 0.0394
largest and mean Δ/σ	0.003, 0.001
max peak in final diff map	0.46 e/Å^3
min peak in final diff map	−0.29 e/Å^3

	[$Fe_{19}(\mu_3$-O)$_6(\mu_3$-OH$(\mu_2$-OH)$_8$(heidi)$_{10}(H_2O)_{12}]^+$ and [$Fe_{17}(\mu_3$-O)$_4(\mu_3$-OH)$_6(\mu_2$-OH)$_{10}$(heidi)$_8(H_2O)_{12}]^{3+}$ plus 4 NO_3^- Anions and 60 Lattice Waters (**2**)
empirical formula	$C_{108}H_{332}Fe_{36}N_{22}O_{226}$
formula weight	3783.2
crystal color, habit	brown, needle
crystal dimensions (mm)	0.10 × 0.15 × 0.36
crystal system	triclinic
lattice parameters	
a	12.693(13) Å
b	18.060(17) Å
c	28.784(15) Å
α	93.66(6)°
β	94.95(6)°
γ	89.88(8)°
volume	6561(10) Å^3
space group	$P\bar{1}$ (No. 2)
Z value	1
D_{calc}	1.916 g cm^{-3}
F(000)	3878
μ(Mo Kα)	1.791 mm^{-1}
radiation	Mo Kα (λ = 0.71073 Å)
temperature	22 °C
scan range (2θ)	2−50°
scan type	ω
index ranges	−15 → 8 *h*, −20 → 20 *k*, −32 → 32 *l*
no. of reflns measd	total 21592 (R_{int} = 0.0965)
	unique 19119
corrections	Lorentz-polarization
	empirical absorption
system used	Siemens SHELXTL PLUS (VMS)
structure solution	direct methods
refinement	full-matrix least-squares
function minimized	$\sum w(\|F_o\| - \|F_c\|)^2$
hydrogen atoms	riding model fixed isotropic *U*
weighting scheme	$w^{-1} = \sigma(F) + 0.0090F^2$
no. observns ($F > 4.00\sigma(F)$)	8252
refln/parameter ratio	9.4:1
residuals: *R*; wR	13.45, 14.24
largest and mean Δ/σ	0.041, 0.002
max peak in final diff map	1.59 e/Å^{-3}
min peak in final diff map	−1.44 e/Å^{-3}

Table 2. Selected Bond Lengths (Å) and Angles (deg) for $[Fe(heidi)(H_2O)]_2$ (**1**)

Fe−O(1)	1.978(3)	Fe−N	2.204(2)
Fe−O(2)	1.970(3)	Fe−FeA	3.119(1)
Fe−O(3)	2.014(3)	Fe−O(3A)	1.937(2)
Fe−O(4)	2.023(3)		
O(1)−Fe−O(2)	152.2(1)	O(2)−Fe−FeA	99.1(1)
O(1)−Fe−O(3)	101.0(1)	O(3)−Fe−FeA	37.0(1)
O(2)−Fe−O(3)	92.0(1)	O(4)−Fe−FeA	136.0(1)
O(1)−Fe−O(4)	85.2(1)	N−Fe−FeA	116.5(1)
O(2)−Fe−O(4)	84.8(1)	O(1)−Fe−O(3A)	104.2(1)
O(3)−Fe−O(4)	171.7(1)	O(2)−Fe−O(3A)	102.7(1)
O(1)−Fe−N	78.4(1)	O(3)−Fe−O(3A)	75.7(1)
O(2)−Fe−N	80.0(1)	O(4)−Fe−O(3A)	97.4(1)
)(3)−Fe−N	79.5(1)	N−Fe−O(3A)	155.2(1)
O(4)−Fe−N	107.4(1)	FeA−Fe−O(3A)	38.7(1)
O(1)−Fe−FeA	106.0(1)	Fe−O(3)−FeA	104.3(1)

with a superconducting magnet and with the possibility of pumping on the sample holder to go below the 4.2 K temperature.

Results

Structure Solution and Refinement of 1. The structure solution and refinement for **1** proceeded without difficulty. The details are given in Table 1. Selected bond distances and angles for **1** are presented in Table 2. The hydrogen atoms of **1** were placed in ideal positions using a riding model with a fixed isotropic *U*.

Description of the Structure of 1. Each dimer unit is produced by inverting the asymmetric unit, {Fe(heidi)(H_2O)}, about a crystallographic inversion center positioned on the centroid of Fe(1), O(3), Fe(1a), O(3a) (Figure 1).

In each dimeric unit two chemically and crystallographically equivalent iron(III) ions are bridged by the deprotonated alkoxyl group of the ligand, O(3) and O(3a). Selected bond lengths and angles are presented in Table 2. The ligand occupies four coordination sites, N(1), O(1), O(2), and O(3), with the fifth being provided by the bridging alkoxyl, O(3a), from the ligand coordinated to the second iron(III) ion and the sixth by a coordinated water O(4). There are large deviations from idealized octahedral geometry with bond angles ranging from 78.4(1)° for O(1)−Fe−N and 107.4(1)° for O(4)−Fe−N.

The Fe---Fe separation in **1** is 3.119(1) Å with the angle of the bridge Fe−O(3)−Fe(A) 104.3(1)°, and the iron alkoxo bond lengths Fe−O(3) = 2.014(3) Å and Fe−O(3A) = 1.937(2) Å, values comparable to those found in other structures of this type.[14-17] As noted in all complexes with this ligand type, the Fe−N bond length, 2.204(2) Å, is significantly longer than the Fe−O(1), O(2), O(3), and O(4) bond lengths, which is attributable to the lower affinity of iron for nitrogen than oxygen.

Structure Solution and Refinement of 2. The difficulties associated with the data collection (see above) are reflected in the relatively high merging *R* value of 9.65%. The structure could be solved using a "brute force" approach in the SHELXS program, i.e., using a large number of direct-methods attempts coupled with an increased number of reflections in the phase refinement and an increased number of E-Fourier cycles. The nitrate counterions could be discerned in difference maps, although there is evidence of site disorder for these. The 60

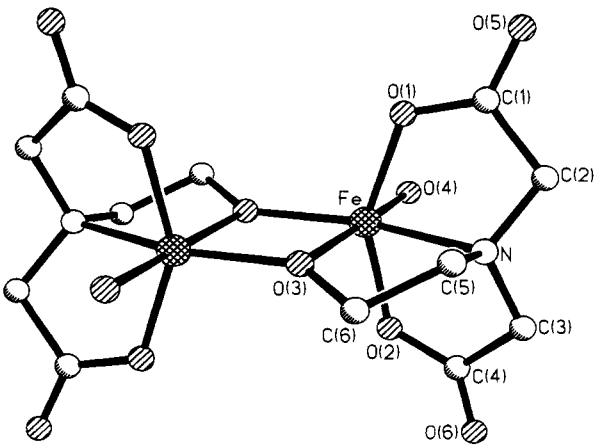

Figure 1. Molecular structure of compound **1**, $[Fe(heidi)(H_2O)]_2$.

waters of crystallization of **2** are very disordered, with evidence for much site disorder and partial occupancies for about 20% of these. Considering the scale of the refinement necessary for this structure, it is clear that a completely satisfactory modeling of the lattice waters will be hard to achieve. In fact, this problem approaches the scale of a refinement of a small protein crystal structure, mainly because of the large amount of associated water. In protein crystal structure determinations, the refinement is often considered complete once about 80% of the water has been modeled (usually in a highly disordered form with large thermal parameters). In this refinement we have located all the water molecules expected from the microanalytical data (performed on C, H, N, and Fe, with O by difference) once the expected amounts of C, H, N, and Fe for the clusters and nitrate counterions have been subtracted. In addition, the final difference map is almost flat with a maximum electron density, found near the central Fe atom of the Fe_{19} cluster, of +1.59 e/Å^3 and minimum of −1.44 e/Å^3. As a result of these constraints, and principally the low scattering efficiency of the crystals, it is not surprising that the refinement did not proceed lower than a conventional *R* value of 13.45% for the 8252 reflections considered observed out of the 19 119 unique data collected. In fact, a lower *R* value could be obtained by omitting more reflections at the expense of the data:parameter ratio (9.4:1). Since this does not result in any changes in the metrical details of the clusters, which are of relevance to the discussion of the magnetic properties of the material, it was deemed preferable to retain the better data:parameter ratio. An improvement in the refinement should be achieved by measuring a low-temperature data set. This should also help in the modeling of the disordered lattice water molecules, although, as stated above, it is unlikely to have any effect on the relative structural details within the clusters themselves. Measuring the data using a more brilliant X-ray source would also be beneficial, mainly in reducing the data-collection time. Full details of the structure solution and refinement are given in Table 1. Selected bond distances and angles for **2** are presented in Table 3. The hydrogen atoms associated with the clusters of **2** were placed in ideal positions using a riding model with a fixed isotropic *U*. The oxo and hydroxo bridges of the two clusters comprising **2** were assigned on the basis of a consideration of geometry at each oxygen: when the bond angles around the oxygen were tetrahedral, the oxygen was assigned as a μ_3-hydroxo, whereas when the angle was trigonal, the oxygen was assigned as a μ_3-oxo. This was confirmed by the microanalytical data and the presence of four nitrate anions in a unit cell containing one molecule of each of the clusters.

Description of the Structure of 2. This structure contains a 19 and a 17 iron cluster which crystallize in the same unit

(14) Kurtz, D. M., Jr. *Chem. Rev.* **1990**, *90*, 585 and references cited therein.
(15) Thich, J. A.; Ou, C. C.; Powers, D.; Vasiliou, B.; Mastropaolo, D.; Potenza, J. A.; Schugar, H. J. *J. Am. Chem. Soc.* **1976**, *98*, 1425 and references cited therein.
(16) Hegetschweiler, K.; Schmalle, H. W.; Streit, H. M.; Gramlich, V.; Hund, H. U.; Erni, I. *Inorg. Chem.* **1992**, *31*, 1299.
(17) Murch, B. P.; Boyle, P. D.; Que, L., Jr. *J. Am. Chem. Soc.* **1985**, *107*, 6728−6729.

Table 3. Selected Bond Lengths (Å) and Bond Angles (deg) for **2**

	Fe–N for Fe_{19}				Fe–O(Alkoxide) for Fe_{19}		
Fe(7)–N(1)	2.196(26)	Fe(9)–N(4A)	2.217(29)	Fe(3)–O(3)	1.957(21)	Fe(10)–O(12)	1.975(22)
Fe(8)–N(2A)	2.164(24)	Fe(10)–N(5)	2.260(30)	Fe(7)–O(8)	2.001(21)	Fe(5)–O(13)	1.977(20)
Fe(6)–N(3)	2.261(30)			Fe(3)–O(9)	1.979(19)	Fe(6)–O(13)	2.005(21)
				Fe(8)–O(9)	1.988(20)	Fe(5)–O(14)	1.998(22)
	Fe–O (Water) for Fe_{19}			Fe(5)–O(12)	1.977(22)	Fe(9)–O(14)	2.023(21)
Fe(5)–O(16)	2.232(23)	Fe(8)–O(24A)	2.079(23)				
Fe(6)–O(19)	2.076(2)	Fe(9)–O(27A)	2.109(24)		Fe–O(Alkoxide) for Fe_{17}		
Fe(7)–O(20)	2.108(21)	Fe(10)–O(30)	2.106(24)	Fe(13)–O(48)	1.972(23)	Fe(16)–O(54)	1.982(30)
				Fe(14)–O(48)	1.988(23)	Fe(1e)–O(54)	2.077(30)
	Fe-μ_2OH for Fe_{19}			Fe(13)–O(50)	2.021(23)	Fe(1e)–O(55)	1.896(24)
Fe(2)–O(6)	1.938(20)	Fe(2)–O(7)	1.981(19)	Fe(15)–O(50)	1.951(24)	Fe(1f)–O(55)	2.059(25)
Fe(7)–O(6)	1.940(19)	Fe(3)–O(7)	1.944(20)				
Fe(4)–O(11A)	1.916(20)	Fe(3)–O(10)	1.980(20)		μ_3OHs for Fe_{19}		
Fe(8)–O(11A)	1.898(19)	Fe(4)–O(10)	2.002(20)	Fe(1)–O(1)–Fe(2)	98.7(7)	Fe(3)–O(2)–Fe(4)	98.5(8)
				Fe(1)–O(1)–Fe(3)	99.2(7)	Fe(1)–O(3)–Fe(4)	101.8(4)
	Fe–N for Fe_{17}			Fe(2)–O(1)–Fe(3)	96.1(7)	Fe(1)–O93)–Fe(2A)	102.8(8)
Fe(15)–N(6A)	2.184(31)	Fe(16)–N(9)	2.178(58)	Fe(1)–O(2)–Fe(3)	99.8(8)	Fe(4)–O(3)–Fe(2A)	94.4(7)
Fe(14)–N(7A)	2.226(30)	Fe(1f)–N(8A)	2.253(28)	Fe(1)–O(2)–Fe(4)	100.4(8)		
					μ_3Os for Fe_{19}		
	Fe–O (Water) for Fe_{17}			Fe(2)–O(4)–Fe(10)	126.9(9)	Fe(5)–O(5)–Fe(6)	99.4(9)
Fe(14)–O(58)	2.062(26)	Fe(1e)–O(62)	2.046(28)	Fe(2)–O(4)–Fe(4A)	102.1(8)	Fe(5)–O(15)–Fe(4A)	119.4(10)
Fe(15)–O(56A)	2.162(25)	Fe(1e)–O(69)	2.077(30)	Fe(10)–O(4)–Fe(4A)	125.6(9)	Fe(5)–O(15)–Fe(9A)	101.3(9)
Fe(16)–O(63)	2.038(33)	Fe(1f)–O(65A)	2.108(31)	Fe(2)–O(5)–Fe(5)	125.0(10)	Fe(4A)–O(15)–Fe(9A)	133.9(10)
				Fe(2)–O(5)–Fe(6)	131.0(11)		
	Fe–μ_2OH for Fe_{17}						
Fe(12)–O(47)	1.972(22)	Fe(1e)–O(46)	1.945(23)		μ_3OHs for Fe_{17}		
Fe(13)–O(47)	1.984(22)	Fe(12)–O(53A)	1.935(21)	Fe(11)–O(42)–Fe(12)	98.8(9)	Fe(13)–O(43)–Fe(17)	97.7(8)
Fe(13)–O(49)	1.991(24)	Fe(15)–O(53A)	1.918(22)	Fe(11)–O(42)–Fe(13)	98.8(8)	Fe(11)–O(44)–Fe(17)	100.9(9)
Fe(17)–O(49)	1.970(21)	Fe(17)–O(51)	1.939(21)	Fe(12)–O(42)–Fe(13)	98.2(9)	Fe(11)–O(44)–Fe(12)	99.6(9)
Fe(12)–O(46A)	1.948(24)	Fe(14)–O(51)	1.913(22)	Fe(11)–O(43)–Fe(13)	101.1(8)	Fe(17)–O(44)–Fe(12)	93.5(8)
				Fe(11)–O(43)–Fe(17)	100.0(9)		
	Fe–O Carboxylate Fe_{19}						
Fe(6)–O(17)	1.999(26)	Fe(8)–O(25A)	1.981(23)		μ_3Os for Fe_{17}		
Fe(6)–O(18)	2.003(24)	Fe(9)–O(28A)	1.960(23)	Fe(17)–O(45)–Fe(12)	101.4(8)	Fe(16)–O(52)–Fe(17)	127.6(13)
Fe(7)–O(21)	1.933(23)	Fe(9)–O(31A)	2.006(21)	Fe(17)–O(45)–Fe(1f)	128.4(11)	Fe(16)–O(52)–Fe(1e)	101.9(11)
Fe(7)–O(22)	1.970(23)	Fe(10)–O(26)	2.001(21)	Fe(12)–O(45)–Fe(1f)	124.7(11)	Fe(17)–O(52)–Fe(1e)	122.7(12)
Fe(8)–O(23A)	2.066(22)	Fe(10)–O(29)	2.027(21)				
					μ_2OHs for Fe_{19}		
	Fe–μ_3O for Fe_{19}			Fe(2)–O(6)–Fe(7)	138.4(11)	Fe(3)–O(10)–Fe(4)	107.9(9)
Fe(2)–O(4)	1.974(17)	Fe(6)–O(5)	1.954(20)	Fe(2)–O(7)–Fe(3)	110.1(9)	Fe(4A)–O(11)–Fe(8A)	141.2(12)
Fe(4)–O(4A)	2.016(18)	Fe(4)–O(15A)	1.912(20)				
Fe(10)–O(4)	1.847(18)	Fe(5)–O(15)	2.031(19)		Alkoxides for Fe_{19}		
Fe(2)–O(5)	1.871(21)	Fe(9)–O(15A)	1.846(20)	Fe(3)–O(8)–Fe(7)	128.8(11)	Fe(5)–O(13)–Fe(6)	96.9(9)
Fe(5)–O(5)	1.956(20)			Fe(3)–O(9)–Fe(8)	129.1(10)	Fe(5)–O(14)–Fe(9A)	96.5(9)
				Fe(5)–O(12)–Fe(10)	125.3(11)		
	Fe–μ_3OH for Fe_{19}						
Fe(1)–O(1)	2.016(17)	Fe(4)–O(2)	2.139(19)		Carboxylate Os for Fe_{19}		
Fe(2)–O(1)	2.209(18)	Fe(1)–O(3)	1.987(18)	Fe(6)–O(17)–C(16)	118.5(23)	Fe(8A)–O(25)–C(12A)	158.8(29)
Fe(3)–O(1)	2.117(17)	Fe(2)–O(3A)	2.115(18)	Fe(6)–O(18)–C(18)	120.2(27)	Fe(9A)–O(28)–C(21)	124.7(25)
Fe(1)–O(2)	2.005(18)	Fe(4)–O(3)	2.116(18)	Fe(7)–O(21)–C(5)	118.3(23)	Fe(9A)–O(31)–C(22)	119.6(24)
Fe(3)–O(2)	2.111(19)			Fe(7)–O(22)–C(4)	115.2(22)	Fe(10)–O(26)–C(28)	127.4(21)
				Fe(8A)–O(23)–C(7A)	115.8(21)	Fe(10)–O(29)–C(26)	120.3(20)
	Fe–O Carboxylate Fe_{17}						
Fe(14)–O(57)	1.938(26)	Fe(16)–O(61)	1.975(35)		μ_2OHs for Fe_{17}		
Fe(14)–O(59)	2.030(23)	Fe(16)–O(68)	1.949(34)	Fe(1e)–O(46)–Fe(12)	127.2(13)	Fe(14)–O(51)–Fe(17)	140.7(11)
Fe(15)–O(60A)	1.973(27)	Fe(1e)–O(64A)	2.030(24)	Fe(12)–O(47)–Fe(13)	107.1(10)	Fe(12)–O(35)–Fe(15)	137.5(12)
Fe(15)–O(66A)	1.985(29)	Fe(1e)–O(67A)	1.948(26)	Fe(13)–O(49)–Fe(17)	107.9(10)		
	Fe–μ_3O for Fe_{17}				Alkoxides for Fe_{17}		
Fe(12)–O(45A)	1.988(20)	Fe(16)–O(52)	1.824(24)				
Fe(17)–O(45)	1.997(19)	Fe(17)–O(52)	1.964(24)	Fe(13)–O(48)–Fe(14)	128.8(12)	Fe(16)–O(54)–Fe(1e)	93.1(12)
Fe(1f)–O(45A)	1.834(19)	Fe(1e)–O(52)	1.970(24)	Fe(13)–O(50)–Fe(15)	127.8(12)	Fe(1e)–O(55)–Fe(1f)	124.3(12)
	Fe–μ_3OH for Fe_{17}				Carboxylate Os for Fe_{17}		
Fe(11)–O(42)	2.044(19)	Fe(17)–O(43)	2.151(21)	Fe(14)–O(57)–C(47A)	120.7(28)	Fe(16)–O(61)–C(51)	117.4(28)
Fe(12)–O(42A)	2.104(22)	Fe(11)–O(44)	1.997(21)	Fe(14)–O(59)–C(45A)	118.1(24)	Fe(16)–O(68)–C(49)	117.8(46)
Fe(13)–O(42A)	2.106(21)	Fe(12)–O(44A)	2.126(20)	Fe(15)–O(60)–C(40)	112.5(30)	Fe(1f)–O(67)–C(32)	120.2(27)
Fe(11)–O(43)	1.977(20)	Fe(17)–O(44)	2.105(22)	Fe(15)–O(66)–C(38)	122.2(27)	Fe(1f)–O(64)–C(31)	119.1(21)
Fe(13)–O(43)	2.103(19)						

cell along with four nitrate anions and 60 waters of crystallization. In view of the obvious difficulties with the nomenclature, these are known colloquially in our laboratory as "Crusts", which stands for cluster rust or captured rust, the latter reflecting the way in which an iron oxyhydroxide mineral has been "caught". The formulae of the two crusts are $[Fe_{19}(\mu_3\text{-}O)_6(\mu_3\text{-}OH)_6(\mu_2\text{-}OH)_8(heidi)_{10}(H_2O)_{12}]^+$ (Figure 2) and $[Fe_{17}(\mu_3\text{-}O)_4(\mu_3\text{-}OH)_6(\mu_2\text{-}OH)_{10}(heidi)_8(H_2O)_{12}]^{3+}$ (Figure 3), and their re-

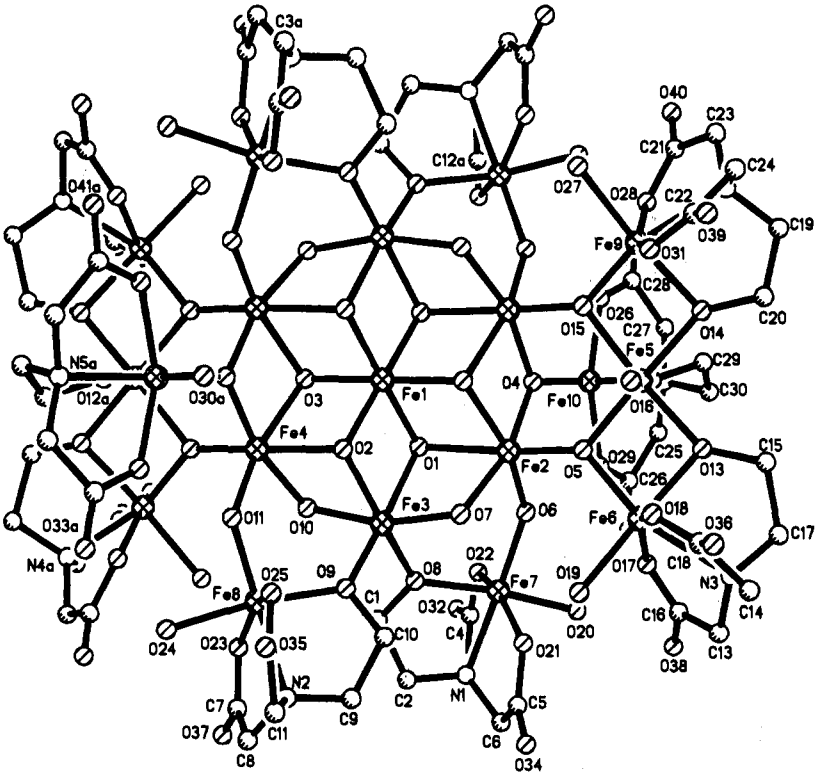

Figure 2. Structure of $[Fe_{19}(\mu_3\text{-}O)_6(\mu_3\text{-}OH)_6(\mu_2\text{-}OH)_8(heidi)_{10}(H_2O)_{12}]^{1+}$, Fe_{19}.

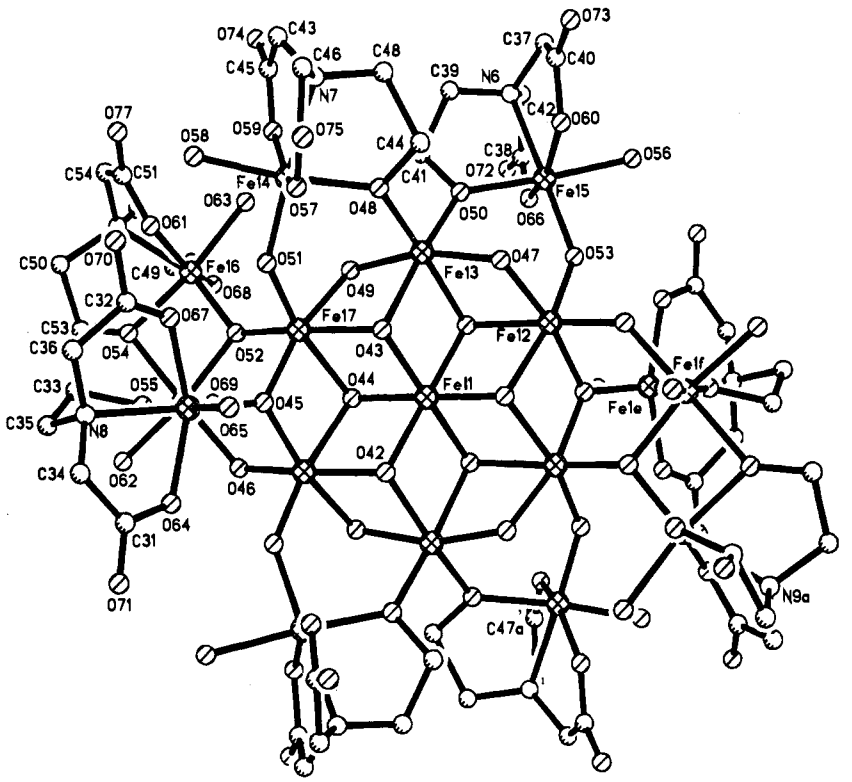

Figure 3. Structure of $[Fe_{17}(\mu_3\text{-}O)_4(\mu_3\text{-}OH)_6(\mu_2\text{-}OH)_{10}(heidi)_8(H_2O)_{12}]^{3+}$, Fe_{17}.

lationship within the unit cell is shown in Figure 4. The central iron atoms of both clusters sit on inversion centers at 0,0,0 and 0.5,0.5,0.5; therefore, the asymmetric unit consists of two half-clusters. The crystal structure can be described as two interpenetrating lattices, one containing the Fe_{17} crusts and the other the Fe_{19}. The structures can be separated into an inorganic core unit $[Fe_7(\mu_3\text{-}OH)_6(\mu_2\text{-}OH)_4\{(\mu_3\text{-}O)Fe\}_2]^{13+}$ (Figure 5a, left) which can be recognized as a portion of an $\{Fe(OH)_2\}_n^{n+}$ lattice consisting of hcp hydroxides with irons in the octahedral holes. The building blocks for this core are $[Fe_3(OH)_4]^{5+}$ units (cubes with one corner iron missing) shown in Figure 5b, right. The core is contained within a shell of iron/heidi units. In the case of the Fe_{19} crust, this central core unit is surrounded by ten iron/heidi units linked to the core by μ_3-O (*e.g.*, O(5)), μ_2-OH (*e.g.*, O(11)) and alkoxo bridges from the heidi (*e.g.*, O(9)) (Figure 2). This gives the outer shell of Fe_{19} the formula $\{Fe_{10}(heidi)_{10}(H_2O)_{12}(\mu_3\text{-}O)_4(\mu_2\text{-}OH)_4\}^{12-}$ and an overall charge on Fe_{19} of 1+. The vacant sites on the peripheral iron centers are

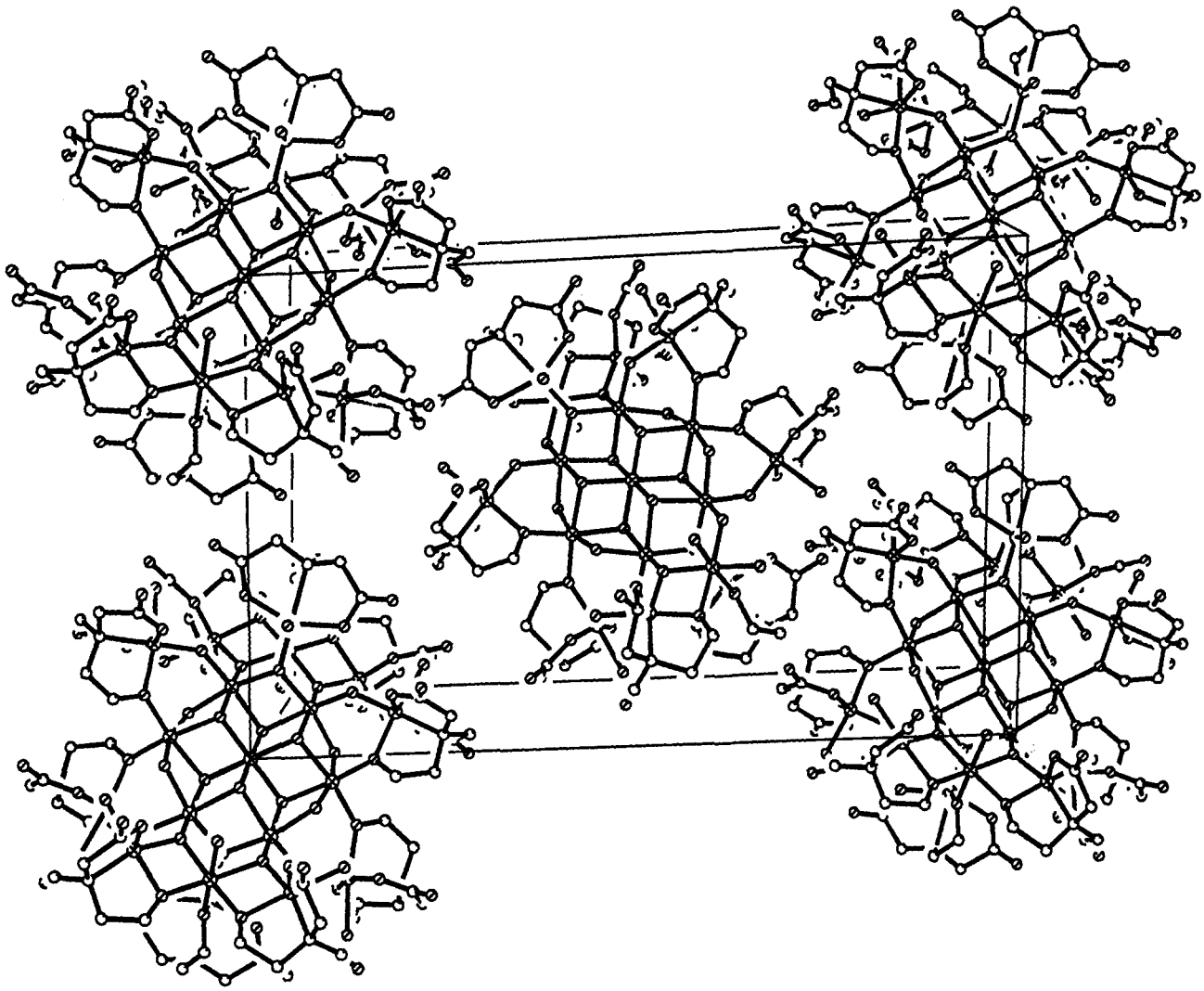

Figure 4. Unit cell of **2** ($Fe_{36}C_{108}H_{332}N_{22}O_{226}$) showing the relationship of Fe_{19} ($[Fe_{19}(\mu_3\text{-}O)_6(\mu_3\text{-}OH)_6(\mu_2\text{-}OH)_8(heidi)_{10}(H_2O)_{12}]^{1+}$) and Fe_{17} ($[Fe_{17}(\mu_3\text{-}O)_4(\mu_3\text{-}OH)_6(\mu_2\text{-}OH)_{10}(heidi)_8(H_2O)_{12}]^{3+}$). Key: cross-hatched, Fe; diagonal lined, O; shaded, C; open circle, N.

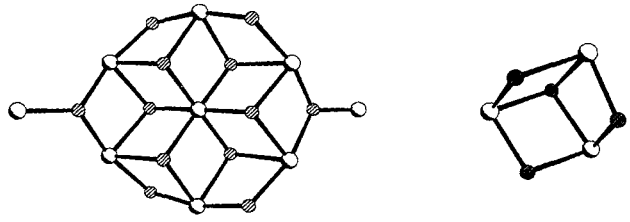

Figure 5. (a, left): $[Fe_7(\mu_3\text{-}OH)_6(\mu_2\text{-}OH)_4\{(\mu_3\text{-}O)Fe\}_2]^{13+}$ core common to Fe19 and Fe17. (b, right): $[Fe_3(OH)_4]^{5+}$ building blocks. Key: shaded, Fe; diagonal lined, O.

taken up with water molecules so that each iron atom is octahedrally coordinated. The Fe_{17} crust is constructed in a similar manner: two symmetry-related Fe/heidi units are absent and consequently two μ_2-OH units replace two of the μ_3-O units in Fe_{19}. The formula of the cluster shell is $\{Fe_8(heidi)_8(H_2O)_{12}(\mu_3\text{-}O)_2(\mu_2\text{-}OH)_6\}^{10-}$, giving Fe^{17} an overall charge of 3+. The two symmetry-related iron/heidi fragments present in Fe_{19} and absent in Fe_{17} correspond to Fe(6) and its partner related by inversion in Fe_{19}. Fe(18) compensates for this missing coordination by sharing ligand alkoxos with Fe(16) and Fe(19), O(54) and O(55), respectively (Figure 3), bridging to the core via one μ_3-O, O(52), and one μ_2-OH, O(40), and having two coordinated waters. The corresponding iron to Fe(18) in Fe_{19}, Fe(5), has only one coordinated water. The rest of its bonding requirements are satisfied by the alkoxos shared with Fe(9), Fe(10), and Fe(6), and it is attached to the central core by two μ_3-O's, O(5) and O(15).

The average iron−iron bond length in the cores of Fe_{19} and Fe_{17} is 3.17 Å with the shortest being 3.08 and the longest 3.22 Å, whereas around the periphery, *e.g.*, Fe(9) to Fe(5) and Fe(5) to Fe(6), they are slightly shorter at 2.99 Å (a full list of Fe−Fe distances is available as supplementary material). The shorter Fe−Fe bond length is a consequence of the more acute angles at the alkoxo bridges Fe(9)−O(14)−Fe(5) and Fe−O(13)−Fe-(6) (96.5(9)° and 96.6(9)°, respectively (Table 3), bringing the iron atoms closer together. The type of bonding illustrated by the heidi ligand on the periphery of these structures, and in particular its ability to connect two iron centres *via* its alkoxide function, is the same as found for compound **1**. The bond lengths and angles do not differ significantly in either compound (Fe−Fe(A) in compound **1** is 3.12 Å), with the exception of the less acute Fe−(O3)−Fe(A) angle in the dimer (104.3(1)°, see Table 2).

As can be seen in Table 3, the iron atoms in **2** are all in distorted octahedral environments and we can distinguish three groups of iron type, namely the purely inorganic iron at the center, the outer irons coordinated to the organic shell, and the irons at the periphery of the core which link between these. This is directly comparable to the situation in ferritin[9] which can also, analogously to crusts, be regarded as a trapped mineral phase contained in an organic shell. In these cases it may be

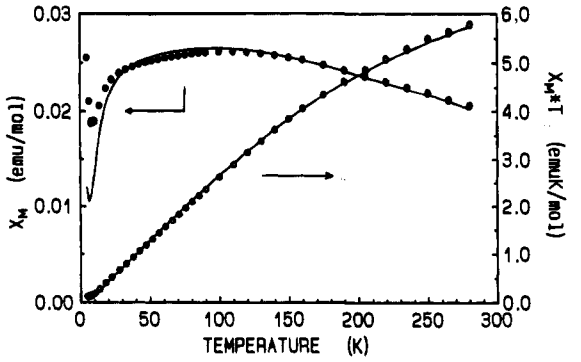

Figure 6. Temperature dependence of the magnetic susceptibility of **1**. The filled circles represent the molar susceptibility for the dimer while the open ones represent the product of the susceptibility with temperature. The solid lines correspond to the best fit values (see text).

possible to identify the mineral type in the core but it must be recognized that this represents a finite portion of an infinite crystal structure and therefore boundary effects will be present. A further consideration in regard to the magnetic properties is the interaction between the crusts in the crystal lattice. Here the mean planes of the cores of the two types of crust are angled at 28.4°, and the distance between the two central irons is 17.229 Å. For the Fe_{19} and Fe_{17} crusts, the closest approach for two central iron ions is 12.693 Å. The whole crystal structure is held together through an extensive and disordered hydrogen-bonded network involving the lattice waters. The extent to which the details of the crystal structure, such as the relative packing of individual crusts, affect the magnetic properties can only be tested by measuring examples which crystallize with different lattice arrangements.

Magnetic Properties and EPR Spectra. The temperature dependence of χ and χT for **1** is shown in Figure 6. The fact that the susceptibility goes through a broad maximum at ca. 100 K is a clear indication of antiferromagnetic exchange interaction within the dimer. Standard analysis indicates the complex has a room-temperature χT value of 5.79 emu mol^{-1} K (4.81 μ_B per iron) which falls to 0.125 emu mol^{-1} K (0.71 μ_B) at 5 K and the data fit well for a J value of 26.8 cm^{-1} (the spin Hamiltonian is used in the form $H = JS_1 \cdot S_2$). The rapid increase of χ below 10 K can be accounted for by the presence of about 2% monomeric impurity.

The extent of antiferromagnetic interaction in alkoxo-bridged dimers is very sensitive to the structural parameters of the bridges, *i.e.*, the Fe−O distances and Fe−O−Fe angles. Lower values are usually observed in dihydroxo-bridged dimers[14] and dialkoxo-bridged dimers,[18] but a larger J value, 30.8 cm^{-1}, was found in $Fe_2(acac)_2(OC_2H_5)_2$ where the structural parameters (Fe−O = 1.98 Å and Fe−O−Fe = 103°) compare well with those of **1**.[19]

The temperature dependence of χT for **2** in the range 2−280 K in an external field of 500 Oe below 80 K is shown in Figure 7. The room-temperature value, 108 emu mol^{-1} K, corresponds to 3 emu mol^{-1} K per iron (4.90 μ_B), clearly pointing to strong antiferromagnetic interactions. On decreasing the temperature, χT steadily increases, reaching a maximum of 218 emu mol^{-1} K at ca. 16 K, and then decreases to 189 emu mol^{-1} K at 3.2 K. The points below 20 K if plotted as χ^{-1} vs T lie on a straight line, as shown in the inset of Figure 7, and can be fitted to a Curie−Weiss law with C = 226.7 emu mol^{-1} K and θ = −0.664 K. The value of C is very high, corresponding to 6.29

(18) Chin-Hua, S.; Rossman, G. R.; Gray, H. B.; Hammond, G. S.; Schugar, H. J. *Inorg. Chem.* **1972**, *11*, 990.
(19) Chiari, B.; Piovesana, O.; Tarantelli, T.; Zanozzi, Z. *Inorg. Chem.* **1984**, *23*, 3398.

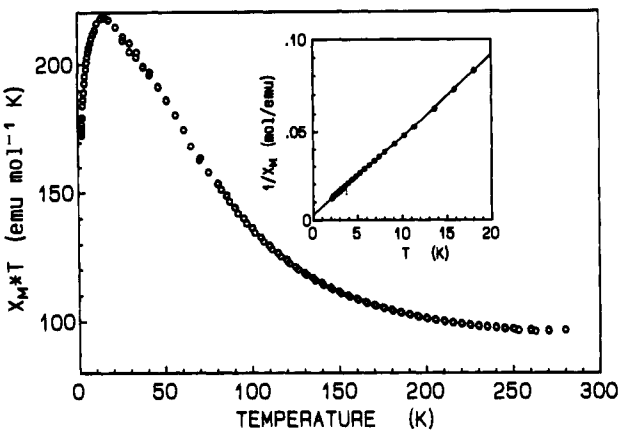

Figure 7. Temperature dependence of χT vs T for Fe_{17+19} in the range 2−280 K. Below 80 K the applied field is 500 Oe. In the inset χ^{-1} is plotted vs T. The solid line represents the best fit values obtained with the Curie−Weiss law (see text).

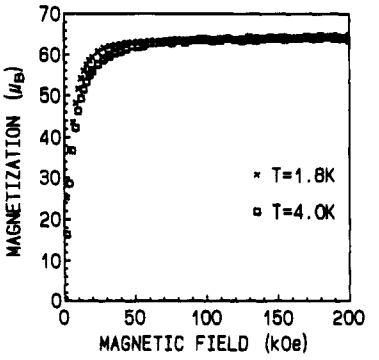

Figure 8. Magnetization curves for Fe_{17+19} at 1.8 K (×) and 4 K (□).

emu mol^{-1} K per iron ion, to be compared to C = 4.375 emu mol^{-1} K for an isolated iron ion.

The ac susceptibility recorded with no applied magnetic field down to 1.5 K is essentially identical to the dc susceptibility, and no out-of-phase component of the susceptibility is observed, indicating that relaxation effects are not relevant in this range of temperatures.

Magnetization measurements were performed at 1.8 and 4 K with external fields reaching 200 kOe. The results are shown in Figure 8. The increase of the magnetization is rather rapid, and no discontinuity is observed. Above 60 kOe the saturation value of 65 μ_B is reached.

Polycrystalline powder EPR spectra were also recorded in the range 4.2−300 K. At room temperature, a broad isotropic signal was observed at g = 2, with peak-to-peak line width of 2400 G, as shown in Figure 9. The signal becomes markedly anisotropic on decreasing the temperature, and the signal shifts to low field. At 4.2 K, the spectrum resembles that of an anisotropic $S = {}^1/_2$ system with $g_\perp \approx 4$, and $g_\parallel$ too broad to be detected.

Attempts were also made to record single crystal EPR spectra, but no suitable individual crystal could be found. Attempts were made to use bunches of iso-oriented small single crystals. Since they are needle shaped, it is relatively easy to orient them parallel to the c axis, while no really good control could be achieved in the perpendicular direction. The spectra show only one broad signal for every crystal orientation. The line width is angle dependent. Reasonably narrow signals are observed when the magnetic field is at 50° from c and the g value approaches 3.3. On moving from this direction the signal broadens, but there is good evidence that the resonance shifts to high field.

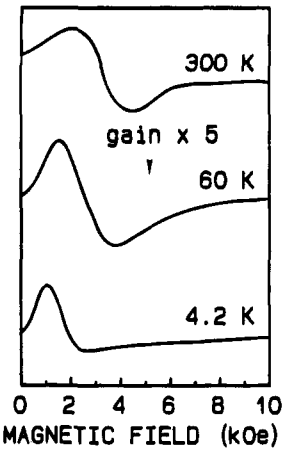

Figure 9. Polycrystalline powder X-band EPR spectra of Fe_{17+19} at 300, 60, and 4.2 K. The $g = 2$ resonates at $H = 3.31$ kOe.

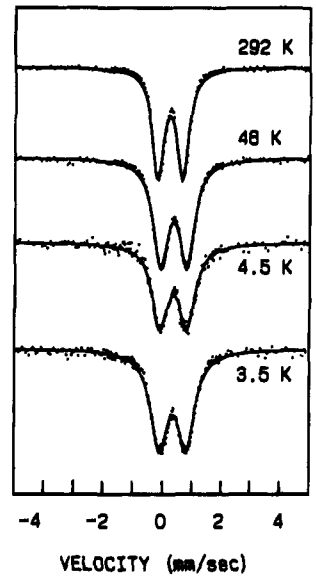

Figure 10. Mössbauer spectra of Fe_{17+19} in zero applied field at four temperatures. From the bottom to the top: 3.5 K, 4.5 K, 48 K, and 292 K.

Mössbauer Spectra. The first series of measurements taken without an external magnetic field consists of eight measurements at temperatures ranging from 300 to 3.5 K (Figure 10), the latter being to check if any magnetic behavior was likely to arise (see for example ref 13). Presumably the rapid motion of the magnetic iron electronic moments causes the quenching of the magnetic hyperfine structure, and all the spectra are doublets. The observed values for the isomer shift, I.S., range from 0.47 mm/s (αFe) at low temperature to 0.36 mm/s at room temperature, RT. The quadrupole splitting decreases with increasing temperature from 0.91 to 0.85 mm/s at RT, values which are characteristic of high-spin iron(III). The line width γ also decreases monotonically with increasing temperature from 0.67 mm/s at 3.5 K to 0.44 mm/s at RT, values which are from three to two times the expected values for a single site, and (or) nonrelaxing case. This line broadening is probably caused by superposition of spectra arising from chemically nonequivalent iron sites. The fact that the broadening increases as the temperature decreases also may be due to the lowering of fast electronic relaxation processes.

The second series consists of measurements at five temperatures from 61 to 4.5 K with a magnetic field of 35 kOe applied parallel to the optical axis (Figure 11). It is clear that the intermediate lines (2 and 5) are almost absent. This behavior

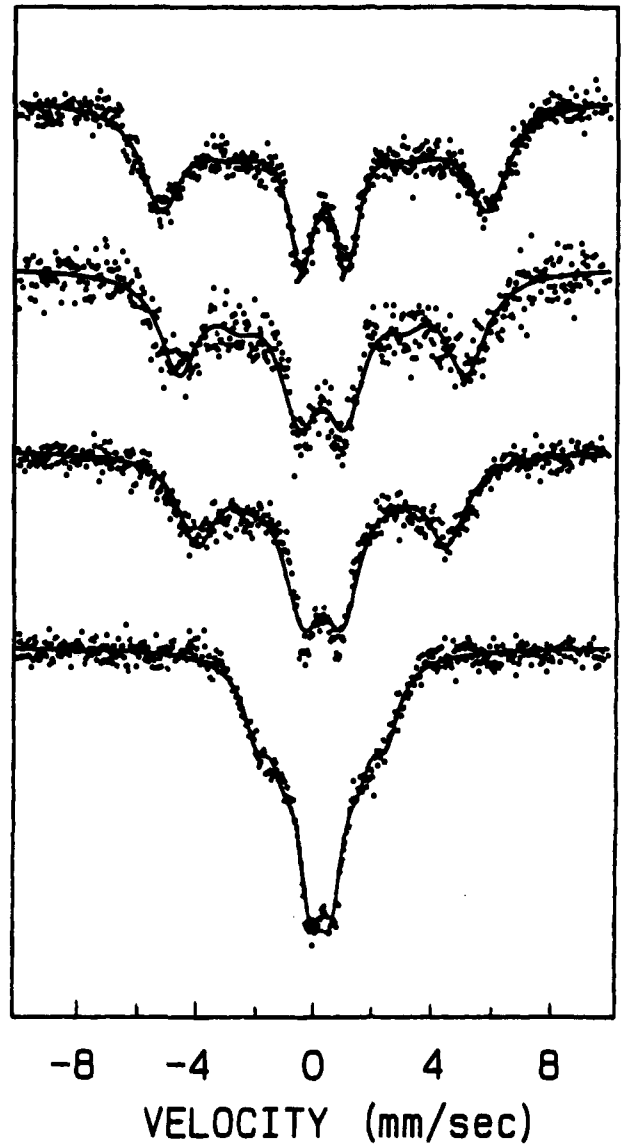

Figure 11. Mössbauer spectra of Fe_{17+19} with an applied field of 3.5 T parallel to the optical axis at four temperatures. From the top to the bottom: 4.5 K, 10 K, 21 K, and 61 K.

is completely different from that observed in other nanometer-sized structures; see, *e.g.*, ref 13, where the spectra recorded in an external magnetic field show a complete six-line profile. The absence of the intermediate lines shows that, in our case, the iron electronic moments and the related hyperfine magnetic field are roughly parallel or antiparallel to the externally applied magnetic field.

Due to the presence of electronic relaxation effects, a correct fitting of the spectra is not straightforward. As a first attempt we make the assumption that the motion of the iron electronic moment, in the external magnetic field, is rapid compared to the Mössbauer time scale. Then the shape of the spectra will depend only on the average value of the hyperfine magnetic field. By fitting the spectra using a sextet, the effective hyperfine field $\langle H_{hf} \rangle$ can be derived, and it is found to decrease as the temperature increases, from 340 kOe at 4.5 K to 135 kOe at 61 K (Figure 12).

Discussion

Synthesis. The species which are important in aqueous solutions of Fe(III) and chelating ligands can be understood in terms of Scheme 1.

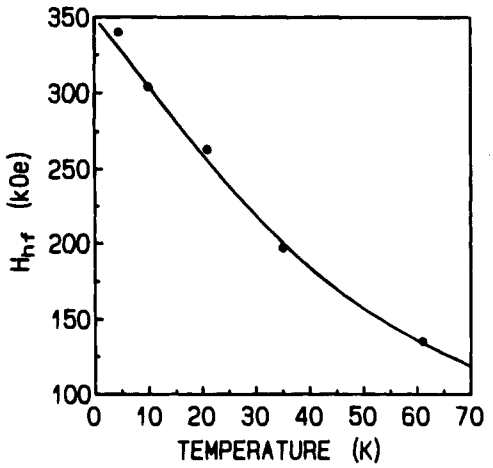

Figure 12. Temperature dependence of the hyperfine field obtained by the Mössbauer spectra of Fe_{17+19} in an applied field. The solid line represent the values calculated with formula 3.

Scheme 1[a]

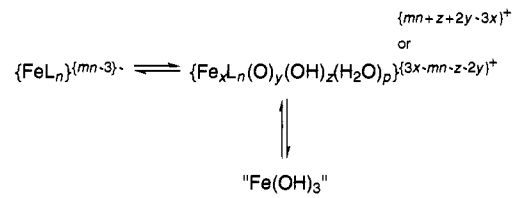

[a] For $[Fe(heidi)(H_2O)]_2$ (**1**), $x = 2$, $n = 2$, and $p = 2$; for $[Fe_{19}(\mu_3\text{-}O)_6(\mu_3\text{-}OH)_6(\mu_2\text{-}OH)_8(heidi)_{10}(H_2O)_{12}]^+$, $x = 19$, $n = 10$, $y = 6$, $z = 14$, and $p = 12$; and for $[Fe_{17}(\mu_3\text{-}O)_4(\mu_3\text{-}OH)_6(\mu_2\text{-}OH)_{10}(heidi)_8(H_2O)_{12}]^{3+}$, $x = 17$, $n = 8$, $y = 4$, $z = 16$, and $p = 12$.

It appears that the two most important parameters operating in the systems studied here are the relative ratio of iron:ligand and the pH gradient, which is governed by the "harshness" of the hydrolyzing species. Obviously these two principal effects work in conjunction with each other as well as with other less important factors in determining the major species forming in the hydrolysis reaction.

When the iron:ligand ratio is such that most of the coordination sites on the metal are taken by the ligand's functional groups, small species result. The ligands block some of the sites available for the coordination of water and thereby inhibit the deprotonation process. An example of this is the monomeric species $Na_3[Fe(nta)_2]\cdot 5H_2O$,[20] which has no coordinated waters. Alternatively they exist as small oligomers, principally dimers. These are often oxo-bridged species such as $Ba[\{Fe(nta)(H_2O)\}_2O]\cdot 4H_2O$.[21] Such oxo-bridged species are likely to be dominant molecules in the early stages of the hydrolysis of iron(III). When the iron:ligand ratio is such that there are plenty of coordination sites available on the iron for water molecules (*i.e.*, when the iron is in excess), aggregated species predominate. These are complicated molecules containing iron oxyhydroxide clusters encapsulated by iron ligand units. An example of these types of species are the Fe_{19} and Fe_{17} clusters.

The pH gradient in a solution will depend in some way on the pK_b of the base.[22] For example, a strong base such as sodium hydroxide will produce a steep pH gradient, while for a weaker base such as pyridine, the gradient will be shallower. The result of this in iron(III) solutions is that strong bases tend to shift the equilibrium, shown in Scheme 1, completely over to the right-hand side, producing "large" or "infinite" species such as iron(III) oxyhydroxide minerals (*i.e.*, "$Fe(OH)_3$" which is a collection of mineral phases). On the other hand, a weaker base will tend to encourage the formation of smaller aggregated species. Under favorable conditions, these can be isolated as molecular species such as the Fe_{19} cluster, corresponding to an intermediate step predominating, *i.e.*, one of the $\{Fe_xL_n(O)_y(OH)_z(H_2O)_p\}^{(mn+z+2y-3x)-}$ species. Thus, the compound **2** can be crystallized from aqueous solution using a variety of weak bases such as pyrrolidine, quinoline, and 1-methylimidazole, as indicated by X-ray powder diffraction (available as supplementary material), comparative IR spectra, and elemental analysis. When strong bases such as NaOH are used, there is no evidence for the formation of **2** at all, although it is still possible to isolate **1**. In view of the high lability of iron(III) high-spin systems, predicting the likely speciation in aqueous solutions is expected to be very difficult. The hydrolytic chemistry of the metal ion complicates efforts to quantify the pH gradient in a solution. It seems reasonable to expect that stronger bases will produce steeper gradients, but it has not yet proved possible to correlate product formation with pK_b of a range of organic bases.

Additional factors such as the dilution and the solubilities of individual species will be relevant to the products which can be isolated. Both **1** and **2** can be isolated in high yields from aqueous solutions. This is partly a result of their low solubility under these conditions, allowing for nucleation and growth to become favorable. It is not possible to say whether the high yields are a result of this inherently low solubility or a reflection of the importance of these species in the solution state without performing solution state measurements. However, solution state measurements such as potentiometry would have to be carried out using conditions rather different from those of the synthetic experiments. Dilution would be much higher and this could lead to different hydrolytic processes becoming important. Also, the presence of dissolved salts in order to maintain constant ionic strength is likely to have an effect on the solubility of the species. Use of other solution state techniques, such as vibrational spectroscopy (ATR-IR), Raman spectroscopy, and visible spectroscopy, can give insights into the likely speciation in reaction solutions of **1** and **2**. We are currently developing an approach to defining solution state speciation using a range of complementary techniques such as these in conjunction with potentiometric measurements in order to ascertain which are the most important species present using the conditions given in the Experimental Section for the synthesis of the two materials.

As might be expected, further changes in the iron:ligand ratio result in different species becoming important. When the amount of iron(III) is further increased, much more soluble species are formed, some of which are stable to pH values above 7.[23] Preliminary microanalytical data on these show that they are likely to contain more iron centers since the amount of iron in a typical sample is ca. 30%, and the carbon content is ca. 10%. Preliminary experiments using related tetradentate ligands, such as H_3nta, indicate that large aggregates can also be synthesized under conditions of high iron:ligand ratio and shallow pH gradient. Since these compounds are not yet structurally characterized, it is not appropriate to discuss them further here except to note that the general synthetic method does appear to follow the trends outlined in Scheme 1.

Infrared Spectroscopy. The infrared spectrum of **1** provides little information on the alkoxide bridging mode as it is masked

(20) Clegg, W.; Powell, A. K.; Ware, M. J. *Acta Crystallogr., Sect. C* **1984**, *40*, 1822.
(21) Heath, S. L.; Powell, A. K.; Utting, H. L.; Helliwell, M. *J. Chem. Soc., Dalton Trans.* **1992**, 305.
(22) Schneider, W.; Schwyn, B. In *Aquatic Surface Chemistry*; Stumm, W., Ed.; Wiley: New York, 1987; pp 165–195.
(23) Goodwin, S. L.; Heath, S. L.; Powell, A. K., unpublished work.

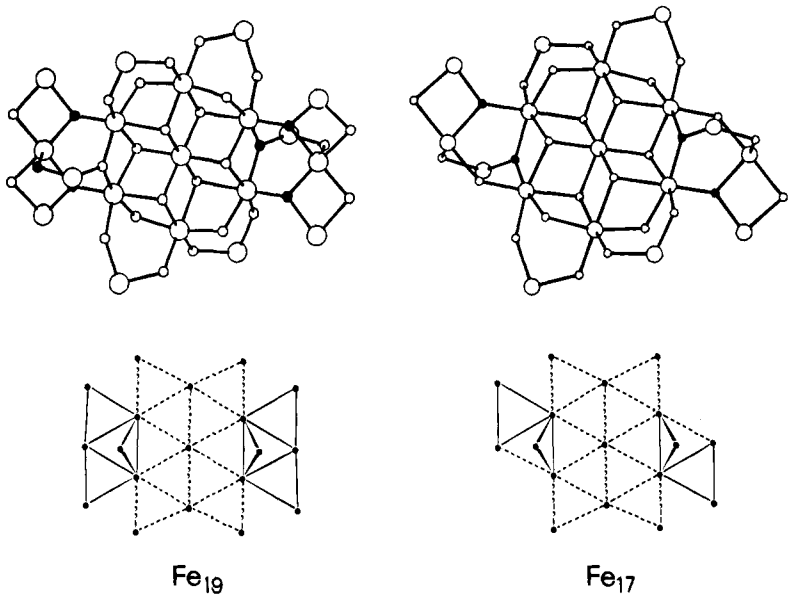

Figure 13. Upper: simplified structures of the two clusters Fe_{19} and Fe_{17}. For the sake of simplicity only oxygen and iron atoms are shown. The oxo ions are represented as full small balls and hydroxo ions as open small balls. Lower: exchange topologies in Fe_{19} and Fe_{17}; (− −) μ-OH or μ-OR, (—) μ-O bridges.

by the presence of strong ligand bands. The bands located at 1620 and 1419 cm^{-1} are assigned to the carboxylate antisymmetric and symmetric stretches. The spectrum of **2** has a broad and strong absorption in the 3800 to 2800 cm^{-1} region which is due to a combination of coordinated and lattice water and bridging-hydroxide stretching modes.[24] The bands occurring in the region of 1650 and 1390 cm^{-1} can be assigned to the carboxylate antisymmetric and symmetric stretching frequencies. The presence of nitrate anions is confirmed by the out-of-plane bending mode, which can be attributed to the sharp peak occurring at 835 cm^{-1}, and the broadening of the carboxylate symmetric stretch due to the ν_3 stretching mode at ca. 1350 cm^{-1}.

Magnetic Properties. The magnetic properties of **2** are a clear indication of a ferrimagnetic behavior. In fact the low value of χT at room temperature indicates the presence of antiferromagnetic interactions, while the high value at low temperature indicates that the preferred spin orientation gives rise to a nonzero component as is observed in ferrimagnets. If we look at the exchange pathways connecting the various metal ions, depicted in Figure 13, we see many triangles, which, in the presence of antiferromagnetic exchange interactions, determine spin frustration effects[25,26] which can stabilize high-spin states and provide many quasi degenerate low-lying states. In Figure 13 we have differentiated oxo bridges from hydroxo and alkoxo bridges because the former are well kwown to produce much more efficient bridges than the latter.[27] Unfortunately, given the large number of spins and the low symmetry of the clusters, it is not possible to perform quantitative calculations on them, and so only qualitative considerations are possible in this case.

The high value of χT reached at low temperature is indicative of the fact that in one or both the Fe_{17} and Fe_{19} clusters, high-spin states are reached. The decrease in χT below 20 K and the fact that the points in the region can be fitted with a Curie–Weiss law with a small θ suggests that weak antiferromagnetic interactions are operative between the clusters. This can be justified by the presence of the waters of crystallization which bridge iron ions from different clusters via hydrogen-bonded oxygen atoms.

In the limit of no interaction between clusters the value of C is given by

$$C = N\mu_B{}^2 g^2[S_1(S_1 + 1) + S_2(S_2 + 1)]/3k \qquad (1)$$

where S_1 and S_2 are the spins appropriate for the Fe_{17} and Fe_{19} clusters, respectively. If the two spins are assumed to be identical, they are calculated to be $S_1 = S_2 = 20.8$.

The saturation magnetization value is expected[27] to be given by

$$M = N\mu_B g[S_1 + S_2] \qquad (2)$$

The highest observed value of M of 65 μ_B for an expected g value of 2 indicates that if $S_1 = S_2$, states as high as 16.5 are lowest in energy. If $S_1 \neq S_2$, one of the two must be even larger. It might be expected that using (1) and (2), the values of S_1 and S_2 could be obtained. However, using the highest value of M, 65 μ_B, and the value of C, no real solution to the problem is found. This could be due to experimental errors and/or to the fact that the ground state in a weak field is different from that in strong fields or to the fact that the appropriate saturation magnetization has not been reached. However, even if we cannot obtain a unique solution to eqs 1 and 2, we can use them to estimate lower limits to S_1 and S_2. In fact we find that in order to minimize the differences between calculated and observed C and M values, one of the S_i values cannot be smaller than $^{33}/_2$. For instance, for $S_1 = {}^{33}/_2$, $S_2 = {}^{27}/_2$ we calculate C = 225.75 emu $mol^{-1}K$ and M = 58 emu $mol^{-1}G$, which are not too far from the experimental values. We can try to rationalize the presence of a ground state with a large spin in terms of the exchange pathways shown in Figure 13. In order to do this we can consider the two clusters in terms of smaller fragments which can be quantitatively treated with the existing theories in order to gain some insight into the mechanism of exchange in Fe_{17} and Fe_{19}. A natural choice of fragments is that of selecting the ions which are bridged by oxo groups. It

(24) Nakamoto, K. *Infrared and Raman Spectra of Coordination Compounds*, 4th ed.; Wiley: New York, 1986.
(25) Vannimenous, J.; Toulouse, G. *J. Phys. C: Solid State Phys.* **1977**, *10*, L537.
(26) McCusker, J. K.; Schmitt, E. A.; Hendrickson, D. N. In *Magnetic Molecular Materials*; Gatteschi, D., Kahn, O., Miller, J. S., Palacio, F., Eds.; Kluwer: Dordrecht, 1991; p 297.
(27) Carlin, R. L. *Magnetochemistry*; Springer-Verlag: Berlin, 1986.

Scheme 2

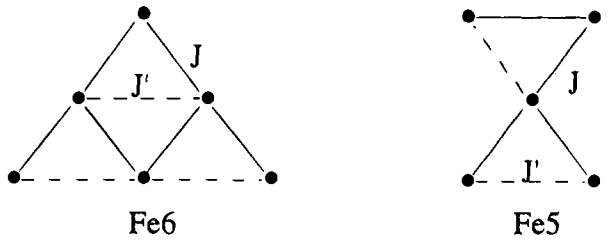

has been shown before that μ-oxo bridges are more effective than μ-hydroxo or μ-alkoxo bridges in transmitting antiferromagnetic interactions between iron(III) ions.[3,14] This is largely a result of the shorter bond lengths between iron(III) and the bridging oxide, probably a result of an increased π-character, although, as Gorun and Lippard observe, this correlation does not hold for unsupported oxide bridges.[28] However, since all the bridges in these clusters count as supported, following the criteria of Gorun and Lippard, this assumption seems a reasonable starting point. Thus, it should be possible to make some prediction on the preferred spin alignment within these subclusters and from these to extrapolate to the whole clusters.

The iron ions which are connected by oxo bridges are localized on the external edges of Fe_{17} and Fe_{19}; there are two groups of six ions in the latter and two groups of five ions in the former. The corresponding exchange topologies are shown in Scheme 2.

On the basis of the available magneto-structural correlations[28] in μ-oxo-bridged iron(III) systems, we can assume at least two different coupling constants for both the Fe_5 and Fe_6 groups, as shown in the scheme. Using two different coupling constants gives a much larger variability of ground states for the two clusters, depending on the J'/J ratio. The spin of the ground state becomes as large as $S = 5$ for Fe_6 at $J'/J = 0.5$. Under the same conditions the ground state of Fe_5 is $S = {}^3/_2$, or $S = {}^5/_2$ for $J'/J = 0.6$. This indicates how a high-spin ground state in Fe_{19} is possible by the assumption that the coupling constants are not all equal to each other. In particular, a possible preferred alignment of the spins is shown in Figure 14. Only the two pairs of iron(III) ions bridged by oxo groups which are connected to the remaining group of seven hydroxo-bridged iron ions are shown in the figure, *e.g.*, Fe2, Fe4a, Fe2a, and Fe4 for Fe_{19}, and we attribute to them the ground state spin of the subgroups of six and five ions for Fe_{19} and Fe_{17}, respectively. Therefore, we assume that each of these pairs of ions conveys an effective spin $S = 5$ for Fe_{19} and either $S = {}^3/_2$ or ${}^5/_2$ for Fe_{17}. If the interaction with the central iron ion (Fe_1 or Fe_{11}) is not frustrated, the two large effective spins orient parallel to each other, and the ground state could be $S = {}^{35}/_2$ for Fe_{19} and either $S = {}^{21}/_2$ or ${}^{25}/_2$ for Fe_{17}.

The conclusion of this analysis is that high-spin ground states are possible for both Fe_{19} and Fe_{17}, provided that the assumptions we used are justified. In addition, the experimental data show that, indeed, in at least one of the two clusters, a high-spin state is achieved. The Mössbauer spectra in zero field show that relaxation is fast down to 3.5 K, and no evidence of a blocking temperature, like that found in superparamagnets, is observed. Magnetically split spectra are often observed in fine particles of iron oxides.[29] From the lack of a similar behavior in Fe_{17+19} clusters, we deduce an upper limit of about 1 K for the energy barrier generated by the magnetic anisotropy between the possible orientations of its magnetic moment.

(28) Gorun, S. M.; Lippard, S. J. *Inorg. Chem.* **1991**, *30*, 1625.
(29) Cianchi, L.; Mancini, M.; Spina, G.; Tang, H. *J. Phys.: Condens. Matter* **1992**, *4*, 2073.

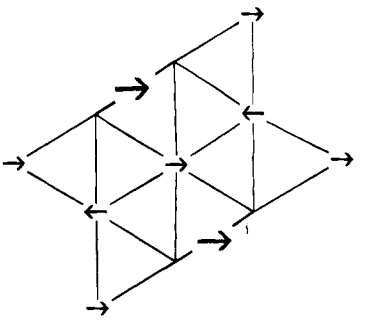

Figure 14. Tentative spin arrangement in the central portion of the clusters.

The Mössbauer spectra, with an applied external field parallel to the γ-ray direction, are characterized by a lack of $\Delta m = 0$ lines. This situation is characteristic of a paramagnet and shows that, in our case, the electronic magnetic moments of all iron atoms are either parallel or antiparallel to each other and to the resulting magnetic moment of the cluster. Assuming that the system behaves as a normal paramagnet in the fast relaxation range, these spectra have been fitted with a sextet. As Figure 11 shows, the spectra are well reproduced and the value obtained for the magnetic field represents the mean effective value for H_{hf}, *i.e.* $\langle H_{hf} \rangle$. Precious information can be obtained by the analysis of the temperature dependence of the $\langle H_{hf} \rangle$ field, shown in Figure 12. $\langle H_{hf} \rangle$ is the component of the hyperfine magnetic field parallel to the γ-ray axis, $\langle H_{hf} \rangle = H_{hf} \langle \cos \theta \rangle$, where θ is the angle between the magnetic moment and the optical axis. Developing $\langle \cos \theta \rangle$ as function of temperature leads to the following expression:

$$\langle H_{hf} \rangle = H_{hf}[1 - kT/MB + 2(e^{-2MB/kT} + e^{-4MB/kT} + ...)] \quad (3)$$

where M is the magnetic moment that can be considered free in the external magnetic field B. The best fit is for $H_{hf} = 350$ kOe and $M = 33\ \mu_B$. It is interesting to note that the value obtained for M is much larger than the iron(III) one ($5\mu_B$) but is in good agreement with the average value per cluster obtained by the saturation magnetization measurements.

Mössbauer spectroscopy is a local probe, and these results suggest that the two clusters do not differ very much in their magnetization. If they did, two hyperfine fields with different temperature dependence would be required to reproduce the experimental spectra. The actual value for the H_{hf} field is proportional to $\langle S \rangle$, the mean value of the magnetic moment and the hyperfine coupling constant A, arising from the sum of several contributions, the most important one being the contact field, which arises from the sum of 2s and 3s contributions. A value of 630 kOe for the contact field of a free Fe(III) ion is suggested for the low-temperature limit, $g\mu_B H \gg kT$.[30] In molecules, H_{hf} has lower values because of covalency effects. The following empirical formula can be used:

$$H_{hf} \approx 630 \delta S/S \quad (4)$$

where δS is the change in the spin of the 3d type due to the charge transfer between metals and ligands and S is the spin of the free ion. The experimental value of 350 kOe for H_{hf} would thus require a large covalent character of the bonding or the presence of a reduced magnetic moment per iron, which will

(30) Vertes, A.; Korecz, L.; Burger, K. *Mössbauer Spectroscopy*; Elsevier: Amsterdam, 1979; p 89.

be the case in the presence of antiferromagnetic exchange interaction within the clusters.[31]

Conclusions

Fe_{17+19} is an example of stabilization of high-spin values in large clusters. Up to now, a ground $S = 14$ state has been proven for a Mn_{10} cluster,[32] $S = 12$ for $[Mn(hfac)_2NITPh]_6$ clusters, containing rings of six manganese(II) and six radicals,[33] $S = 10$ for a Mn_{12} cluster comprising eight manganese(III) and four manganese(IV),[34] and $S = 9$ for a cluster comprising eight iron(III) ions.[4] The indications we obtained from the analysis of the experimental data are that in at least one of the clusters the ground state cannot be smaller than $S = {}^{33}/_2$. If this is confirmed it corresponds to the largest spin ground state so far observed in a molecular cluster.

Except for $[Mn(hfac)_2NITPh]_6$, where the large ground spin state is determined by the antiferromagnetic interaction between $S = {}^5/_2$ and $S = {}^1/_2$ regularly alternating in a ring, in all the other cases the high-spin states originate as a result of conflicting antiferromagnetic interactions between large spins triangularly connected. It is worth noticing that in large clusters containing only $S = {}^1/_2$ spins, the ground state has always been found to possess a small spin.[35] When the individual spins are large, they are much more subject to spin frustration effects and can find many different relative orientations which could produce a large resultant ground spin state. However, the presence of spin frustration does not allow one to predict the ground state of clusters by setting the various coupled spins either up or down. Therefore, for the moment, we do not see a real possibility to suggest simple rules which, given the structures of the clusters, can easily provide the preferred spin alignment at low temperature. In fact, the structure of the central core of iron ions present in both Fe_{17} and Fe_{19}, $\{Fe(OH)_2\}_n^{n+}$, is related to that of goethite, $\{\alpha FeO{\cdot}OH\}$, with the substitution of one OH group with an O group. Goethite behaves as an antiferromagnet, but the magnetic properties of the $\{Fe(OH)_2\}_n^{n+}$ lattice are not known and cannot be known. In goethite, the oxides hydrogen bond to the hydroxides of the next layer, essentially making this a three-dimensional structure, but our lattice type, $\{Fe(OH)_2\}_n^{n+}$, is a layer structure, *i.e.*, two-dimensional, and this will presumably affect magnetic interactions. Also, because it is only a finite portion of this lattice, there are boundary effects. It could be the presence of the Fe_5 and Fe_6 clusters on the edges of Fe_{17} and Fe_{19}, respectively, which tends to stabilize the high-spin states found.

Another important point in the investigation of the magnetic properties of high nuclearity spin clusters is to recognize when the behavior usually associated with infinite assemblies of spins is observed in finite clusters. Anomalous behaviors have been observed in some systems, namely Mn_{12} which comprises eight manganese(III) and four manganese(IV), Fe_{12}, and Fe_{17+19}. In Mn_{12}, large magnetization relaxation effects were observed without any applied magnetic field in an ac susceptibility measurement. We attributed that behavior to the large anisotropy in the ground state, which can be experimentally proven by the EPR spectra. The ac susceptibility measurements on the Fe_{17+19} did not provide any evidence of anomalous behavior, in agreement with the much lower magnetic anisotropy evidenced by the EPR spectra. However, the spectra do reveal some initial anisotropy effect, with the buildup of internal fields. Both anomalous behaviors observed so far have something to do with spin dynamics, and it may be reasonably anticipated that it is in this field that other anomalies can be expected to be observed in large clusters.

The synthetic method presented here will enable us to trap different size portions of this same lattice and also, by varying the properties of the ligands, to isolate clusters of different dimensions. In this way it will be possible to develop our understanding of the magnetic properties of cluster compounds.

Acknowledgment. We are indebted to Prof. M. Guillot of the Service Nationale des Champs Intenses-C.N.R.S. Grenoble, France for the magnetization measurements in a high magnetic field and to Mr. Stephen Bennett, School of Environmental Sciences at the University of East Anglia, for the powder diffraction data. The financial support of MURST and Progetto Finalizzato Materiali Speciali per Tecnologie Avanzate and the S.E.R.C. is gratefully acknowledged.

Supplementary Material Available: Tables of positional parameters and U(eq) for all atoms, anisotropic thermal parameters for all non-hydrogen atoms, and interatomic distances and angles for **1**; tables of positional parameters and U(eq) for all atoms, anisotropic thermal parameters for iron–hydrogen atoms, and interatomic distances and angles for **2**; table of X-ray powder diffraction peaks for **2** prepared using different bases along with **1** for comparison (22 pages). This material is contained in many libraries on microfiche, immediately follows this article in the microfilm version of the journal, can be ordered from the ACS, and can be downloaded from the Internet; see any current masthead page for ordering information and Internet access instructions.

JA9404882

(31) Girerd, J.-J.; Papaefthymiou, G. C.; Watson, A. D.; Gamp, E.; Hagen, K. S.; Edelstein, N.; Frankel, R. B.; Holm, R. H. *J. Am. Chem. Soc.* **1984**, *106*, 5941.

(32) Caneschi, A.; Gatteschi, D.; Laugier, J.; Rey, P.; Sessoli, R.; Zanchini, C. *J. Am. Chem. Soc.* **1988**, *110*, 2795.

(33) Caneschi, A.; Gatteschi, D.; Sessoli, R.; Barra, A. L.; Brunel, L. C.; Guillot, U. *J. Am. Chem. Soc.* **1991**, *113*, 5871.

(34) Sessoli, R.; Gatteschi, D.; Caneschi, A.; Novak, M. A. *Nature* **1993**, *365*, 141.

(35) Gatteschi, D.; Pardi, L.; Barra, A. L., Müller, A. *Polyoxovanadates: the Missing Link Between Simple Paramagnets and Bulk Magnets?*; Müller, A., Pope, M. T., Eds.; Kluwer: Dordrecht, 1993.